Quantitative Analysis of Scanning Force Microscopy Data Using Harmonic Models

Klaus Schröter, Albrecht Petzold, Thomas Henze, and Thomas Thurn-Albrecht*

Institut für Physik, Martin-Luther-Universität Halle-Wittenberg, 06099 Halle, Germany

Received November 1, 2008; Revised Manuscript Received December 12, 2008

ABSTRACT: Starting from established concepts that describe the dynamics of the cantilever in a scanning force microscope operated in intermittent contact mode as that of a driven harmonic oscillator, we introduce effective interaction parameters based on Fourier coefficients to describe the interaction forces. These interaction parameters are linear in the forces and separate conservative from dissipative contributions. They allow a qualitative description of the interaction process and enable a thorough discussion of the influence of experimental parameters on the measured data. Exemplary force spectroscopy data obtained from hard and soft polymeric model surfaces show that consistent data for the interaction parameters can be obtained which can be related to the material properties of the investigated surfaces. Images obtained in intermittent contact mode from a semicrystalline polymer as an exemplary nanostructured surface with hard−soft contrast illustrate that with the approach a clear identification of harder and softer domains is possible.

Introduction

Atomic force microscopy (AFM) or scanning force microscopy (SFM) is nowadays routinely used to measure the topography or to characterize the structure of heterogeneous surfaces on the nanometer scale.[1,2] Especially for heterogeneous polymer systems local variations of mechanical properties and interaction forces can be used for image contrast allowing e.g. to image the surface structure of semicrystalline polymers or microphase-separated block copolymers. Very common for the investigation of polymer surfaces is the intermittent contact mode, also called amplitude modulation (AM) or tapping mode, in which the tip oscillates vertically with its zero position above the sample and only touches the surface during part of the oscillation period. Two common experiments can be distinguished, namely force spectroscopy and imaging. In force spectroscopy the lateral position of the tip on the sample and the excitation amplitude are kept constant, and amplitude and phase of the oscillation are measured while the distance to the sample is varied. For imaging the cantilever tip scans over the surface with fixed excitation, and the height above the sample is adjusted by a feedback loop such that the amplitude of the oscillation is kept at a fixed fraction of the free amplitude. Measured image parameters are height and phase, giving as mentioned above qualitative information about local topography and changes in material properties on a mesoscopic scale. While on the atomistic scale a thorough description of the tip−sample interaction also including simulations is common for the interpretation of images,[3,4] on the mesoscopic scale, which is most relevant for AFM application in polymers, qualitative insight is mostly gained directly from height and phase images, and in general macroscopic continuum models are used to model the tip−sample interaction. The exact relation though between material properties and topography on one side and amplitude and phase on the other side is complicated for several reasons. First, several different interactions contribute, e.g. van der Waals forces, elastic repulsion due to deformation, viscoelastic damping, and adhesion.[5] All these forces typically depend on the tip−sample distance in a nonlinear way. Additionally, the interaction between tip and sample depends on experimental parameters like e.g. cantilever stiffness, amplitude, and frequency of the excitation. Therefore, phase images are mostly used as they are, i.e., without further even qualitative interpretation of the underlying interaction. Also, height images have to be interpreted with care, since during scanning the tip partially indents the surface with the amount of indentation again depending on a combination of experimental parameters and "softness" of the sample surface.[6−8] Hence, in general, height and phase images mix up topography and material contrast, a fact which is often neglected. Only in recent years a quantitative understanding and analysis of AFM data is emerging, enabling a reconstruction of the interaction forces.[5,9−16] In some cases numerical simulations of the motion of the cantilever for given interaction model forces are performed.[17,18] This approach allows detailed studies of cantilever dynamics but in general does not give easily and generally applicable relations between forces and measured parameters. An important simplification is obtained with the so-called harmonic approximation reviewed below.[12]

The purpose of this paper is to add to this development by formulating a simple relation between measured parameters and integral interaction forces with the aim to gain a better understanding of image contrast in force microscopy on common polymer systems. Starting from the insight that under normal conditions in intermittent contact AFM it is just the first Fourier component of the interaction force which contributes to the measured parameters, we introduce effective interaction parameters, which can be calculated from amplitude and phase signals. This approach allows the separation of elastic and dissipative contributions of the interaction forces and a thorough discussion of the role of experimental parameters like cantilever stiffness, excitation amplitude, excitation frequency, and set point in imaging. From the effective interaction parameters one can qualitatively conclude on material properties which allows to identify different phases in the AFM images. We present and discuss exemplary measurements on polymeric model surfaces for both force spectroscopy and imaging.

Theory

Mathematical Description of Cantilever Dynamics by Harmonic Models. Usually, the description of the dynamics of the cantilever of an atomic force microscope starts with the differential equation of a driven harmonic oscillator[5]

* Corresponding author. E-mail: thomas.thurn-albrecht@physik.uni-halle.de.

10.1021/ma8024464 CCC: $40.75 © 2009 American Chemical Society
Published on Web 01/28/2009

$$m\ddot{z} + \alpha\dot{z} + kz = F_0 \cos(\omega t) + F_{ts}(t) \quad (1)$$

Here $z(t)$ is the instantaneous displacement of the cantilever tip from its zero position (Figure 1), m the vibrating mass, k the bending stiffness of the cantilever, and α the damping constant. F_0 and ω are the amplitude and angular frequency of the external driving force, respectively. F_{ts} contains all the tip−sample interaction forces. Equation 1 already contains an approximation, as the three-dimensional vibrating cantilever is described by a point mass attached to a spring. Since in most applications only the fundamental resonance of the cantilever is used and other resonances of the solid structure are irrelevant, this approximation poses no serious problem.[19,20] Additionally, it is assumed in eq 1 that the driving force acts directly on the tip, whereas in reality tips are excited by a dither piezo at the clamped end. It can be shown numerically and experimentally that both methods are equivalent for the case of small damping.[21]

Using eq 1 to interpret AFM measurements requires a relation between the tip−sample forces F_{ts} and the quantities usually measured in an AFM, namely amplitude and phase of the cantilever oscillation at the driving frequency. The interaction forces F_{ts} are highly nonlinear functions of the tip position $z(t)$ and possibly the velocity $\dot{z}(t)$.[5,22] If special mathematical models are assumed for F_{ts}, then the nonlinear differential equation (1) can be solved numerically,[17,18] but this approach alone does not give the desired simple relations between measured quantities and interactions. Unless the nonlinearities are very strong leading to chaotic dynamics, the cantilever motion $z(t)$ and therefore also $F_{ts}(t)$ will be periodic but will of course contain higher harmonics. In common experiments only amplitude and phase at the fundamental driving frequency are measured. Combining data obtained at different distances in force spectroscopy measurements, force−distance curves can be reconstructed under some assumptions. Lee and Jhe[10] explored the case of conservative forces. Hoelscher[12] calculated F_{ts} under the assumption of short contact times and hard substrates. A more general approach was described by Hu and Raman.[16] Experimental approaches to distinguish between different mechanisms of surface interaction based on the analysis of energy dissipation curves were in most cases restricted to hard surfaces.[9]

A qualitative and quantitative understanding of the cantilever motion can be achieved by an analytical treatment of a simplified version of eq 1, the so-called harmonic model. This approximation was also used in the reconstruction algorithms mentioned above.[12,16] In this model a driven harmonic oscillator experiencing only weak additional nonharmonic forces is considered. This approach is analogous to a perturbation theory. The functional form of the solution of the differential equation with perturbation is kept from the differential equation without perturbation while the parameters of the solution are adjusted according to the perturbation. Correspondingly, one assumes that also under the influence of F_{ts} the solution $z(t)$ retains its sinusoidal shape. We assume

$$F(t) = F_0 \cos(\omega t - \varphi) \quad \text{and} \quad z(t) = a \cos \omega t \quad (2)$$

where a is the amplitude of the resulting oscillation and $F(t)$ the external driving force, with the phase difference φ between the two assigned here for simplicity to the excitation. The differential equation (1) now becomes

$$ma\frac{d^2}{dt^2}\cos \omega t + \alpha a\frac{d}{dt}\cos \omega t + ka \cos \omega t = F_{ts}(t) + F_0 \cos(\omega t - \varphi) \quad (3)$$

For F_{ts} a Fourier expansion can be performed

$$F_{ts} = \frac{a_0}{2} + a_1 \cos \omega t + a_2 \cos 2\omega t + ... + b_1 \sin \omega t + b_2 \sin 2\omega t + ... \quad (4)$$

with

$$a_n = \frac{2}{T}\int_0^T F_{ts}(t) \cos(n\omega t)t \quad (5)$$

and

$$b_n = \frac{2}{T}\int_0^T F_{ts}(t) \sin(n\omega t)\, dt \quad (6)$$

Within the harmonic approximation only the first Fourier components ($n = 1$) are kept. From the differential equation (3) we then get

$$a \cos(\omega t)\left[-m\omega^2 + k - \frac{a_1}{a}\right] - a\omega \sin(\omega t)\left[\alpha + \frac{b_1}{a\omega}\right] = F_0 \cos \omega t \cos \varphi + F_0 \sin \omega t \sin \varphi \quad (7)$$

The influence of the tip sample forces enters via the Fourier coefficients a_1 and b_1 in such a way that they can be incorporated as tip−sample contributions k_{ts} and α_{ts} into new effective interaction parameters.

$$k_{eff} = k - \frac{a_1}{a} = k + k_{ts} \quad (8)$$

$$\alpha_{eff} = \alpha + \frac{b_1}{a\omega} = \alpha + \alpha_{ts} \quad (9)$$

with

$$k_{ts} = -\frac{2}{aT}\int_0^T F_{ts}(t) \cos(\omega t)\, dt \quad (10)$$

$$\alpha_{ts} = \frac{1}{a\pi}\int_0^T F_{ts}(t) \sin(\omega t)\, dt \quad (11)$$

Using eq 2, eq 10 can also be written as

$$k_{ts} = -\frac{2}{a^2 T}\int_0^T F_{ts}(t)\, z(t)\, dt = -\frac{2}{a^2}\langle F_{ts} \cdot z \rangle \quad (12)$$

Please note that k_{ts} is not the momentary force gradient of F_{ts} at any time t during the oscillation but an effective value averaged over the whole oscillation cycle. The same applies to α_{ts}. The force gradient k_{ts} is linear in the interaction force F_{ts}, and hence attractive and repulsive force contributions which the tip experiences during the oscillation just add up linearly. This point will strongly simplify the discussion below. A similar description of the tip−sample interaction as the one introduced here was recently used for the reconstruction of force distance curves.[16,23]

Solving eq 7 gives an approximate solution of eq 3, which consists of the well-known steady-state resonance curves of a driven harmonic oscillator for amplitude and phase shift, with the only modification that k and α are replaced by k_{eff} and α_{eff}, respectively.

$$a(\omega) = \frac{F_0/m}{\sqrt{(\omega^2 - \omega_0^2)^2 + (\omega\omega_0/Q)^2}} \quad (13)$$

$$\varphi(\omega) = \arctan\left(\frac{\omega\omega_0/Q}{\omega^2 - {\omega_0}^2}\right) \tag{14}$$

where the resonance frequency ω_0 and the quality factor Q are related to the parameters k_{eff} and α_{eff} by

$${\omega_0}^2 = \frac{k_{\text{eff}}}{m} \tag{15}$$

$$Q = \frac{\omega_0}{\alpha_{\text{eff}}/m} \tag{16}$$

Figure 2 shows schematically the frequency dependence of $a(\omega)$ and $\varphi(\omega)$.

Discussion of the Effective Interaction for a Specific Numerical Example. As we will demonstrate, the description of the tip−sample interaction in terms of the parameters k_{ts} and α_{ts} can be used to describe and analyze the results of AFM force spectroscopy as well as AFM imaging. Generally, while approaching the surface the tip will always sense the attractive interactions first. After direct contact repulsive contributions appear. To develop a more detailed understanding for the way how the different parts of the interaction contribute to the effective interaction parameters, the situation is analyzed at first for a specific model of the interaction.

To demonstrate the typical time dependence of all functions given above we simplify the real forces[22] and assume a conservative force F_{ts} with two contributions.[23] First there is an attractive van der Waals term

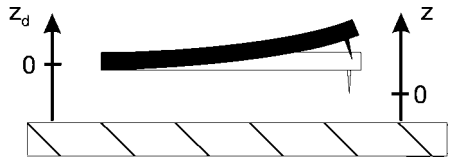

Figure 1. Coordinates used to describe the dynamics of the cantilever. The cantilever is driven by moving z_{d}; its deformation is described by $z(t)$.

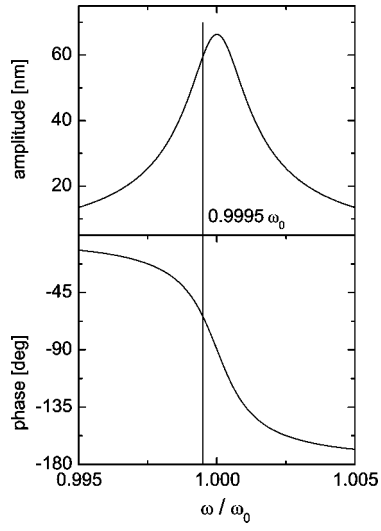

Figure 2. Theoretical dependence of the amplitude a and phase φ of a damped harmonic oscillator on excitation frequency. The parameters correspond to the cantilever 1 (see Table 1).

$$F_{\text{attr}} = -\frac{A_{\text{H}}R}{6d^2} \tag{17}$$

with A_{H} the Hamaker constant, R the tip radius, and d the actual distance between tip and surface. The second contribution is a repulsive force according to the DMT-M (Derjaguin, Muller, Toporov, and Maugis) theory[5] with the typical dependence of the force on the 1.5th power of the indentation into the surface. The surface is located at $z = -z_0$ from the zero position of the oscillating cantilever. Additionally, to avoid the divergence of the attractive force for $d = 0$, a molecular distance d_0 is introduced as a minimal distance. This gives as a whole for F_{ts}

$$F_{\text{ts}} = \begin{cases} -\dfrac{A_{\text{H}}R}{6(z + z_0 + d_0)^2}, & \text{for } z > -z_0 \\ \dfrac{4}{3}E\sqrt{R}(-z - z_0)^{3/2} - \dfrac{A_{\text{H}}R}{6{d_0}^2}, & \text{for } z < -z_0 \end{cases} \tag{18}$$

E is the effective modulus of tip and sample surface. Figure 3 shows the resulting force curve for exemplary parameters.

To give an impression of the time dependence of $F_{\text{ts}}(t)$ and the corresponding integrand in eqs 10 and 11, both were calculated for a given amplitude $a = 60$ nm and a fixed distance z_0 for three different values of the modulus E, namely 10^7, 10^8, and 10^9 Pa. Figure 4 shows the time dependence of the force during one oscillation cycle. For most of the time the tip is so far away from the surface that the force is negligible. Only close to the lower turning point ($\omega t = \pi$) the force F_{ts} assumes noticeable values. For higher values of E an increasing repulsive contribution adds up to constant attractive contribution. Figure 5 shows the time dependence of the integrand of eq 10 for one oscillation period for the same parameters. Both figures look very similar (beside of a change in sign) because the force F_{ts} reaches noticeable values only close to the minimum of the oscillation where $z(t)$ is approximately constant. The elastic tip−sample interaction parameter k_{ts} is given by the integral over the curve in Figure 5; attractive and repulsive contributions simply add up. For a modulus of 10^9 Pa the integral is negative, i.e., k_{ts} positive (repulsive interaction dominates). For 10^8 Pa the integral nearly vanishes, and for 10^7 Pa k_{ts} gets negative (attractive interaction dominates).

Changes in the height z_0 of the tip above the surface lead to similar variations of k_{ts}. An exemplary case with fixed oscillation amplitude, $a = 60$ nm, and different values z_0 of 50, 54, and 58 nm for a sample with modulus $E = 10^8$ Pa are shown in Figures 6 and 7. For decreasing z_0 the tip touches the surface for a larger fraction of the oscillation period, and the attractive contribution to the integral increases slightly. At the same time the repulsive contribution, i.e., the positive contributions in Figure 6, increases strongly. This is caused by the increasing indentation.

Figure 8 shows the time dependence of the integrand in eq 11 used to calculate the additional effective damping contribution α_{ts}. The parameters are the same as in Figures 6 and 7. The integrand shows an antisymmetric shape around the position $\omega t = \pi$ because of the sine function in the integrand. Accordingly, the integral vanishes, in correspondence to the fact that F_{ts} is conservative (cf. eq 18). If $F_{\text{ts}}(t)$ contains dissipative contributions and depends not only on $z(t)$ but also on $\dot{z}(t)$,[10] the time dependence of $F_{\text{ts}}(t)$ will be no more symmetrical to $\omega t = \pi$, resulting in a finite contribution α_{ts}.

Of course, these calculations do not describe directly the measurements in force spectroscopy experiments, in which the average distance between tip and sample is varied. In the calculations above the oscillation amplitude is fixed, and accordingly in a real experiment one would have to vary the excitation amplitude. On the other hand, in the normal experi-

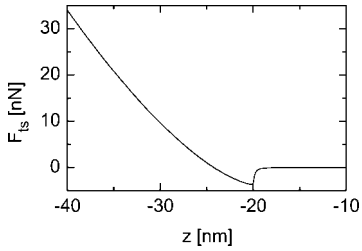

Figure 3. Static force−distance curve (eq 18) for $A_H = 2 \times 10^{-19}$ J, $R = 10$ nm, $z_0 = 20$ nm, $d_0 = 0.3$ nm, and a modulus of $E = 10^8$ Pa. Note the attractive region close to the surface at $z = -20$ nm and the increasing repulsive contribution for larger indentations.

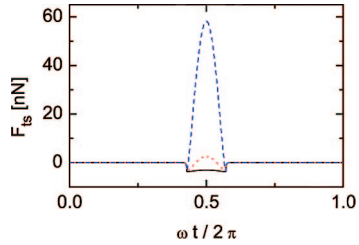

Figure 4. Time dependence of the force F_{ts} for three different values of the effective modulus E (10^7 (solid), 10^8 (dotted), and 10^9 Pa (dashed line)). The oscillation amplitude was chosen as 60 nm; the mean distance of the cantilever from the surface was 54 nm (other parameters as in Figure 3).

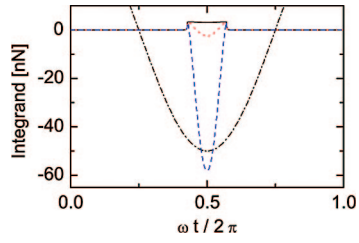

Figure 5. Time dependence of the integrand of eq 10 during one oscillation period. The dash-dotted line shows the relevant part of cos $\omega t \sim z(t)$ for comparison.

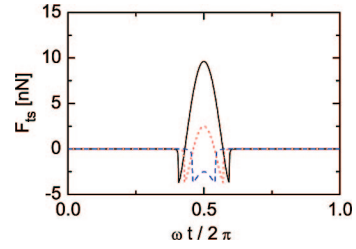

Figure 6. Time dependence of tip−sample force F_{ts} during one oscillation period for a fixed amplitude of $a = 60$ nm and different mean distances z_0 from the surface (50 (solid), 54 (dotted), and 58 nm (dashed line)).

ment the excitation is fixed, and with a change in interaction between tip and sample the oscillation amplitude will vary in such a way that the new interaction parameters k_{ts} and α_{ts} give self-consistently the new oscillation amplitude a. Practically, this means that one would have to calculate the amplitude a iteratively from the equations given above, which is not the aim here. A simple example which can be solved directly is the limit of a tip interacting with a very hard repulsive surface without attractive interaction. $F_{ts}(z)$ is then zero for $z > -z_0$ and very large otherwise. The hard surface will practically limit the oscillation, $a \approx z_0$, and additionally $\alpha_{ts} = 0$. If we assume a high-quality factor (cf. discussion below), then the solution will still be approximately sinusoidal. The force F_{ts} will consist

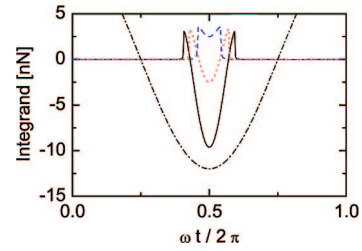

Figure 7. Time dependence of the integrand of eq 10 during an oscillation period for the same parameters as in Figure 6. The dash-dotted line shows a cosine function for comparison.

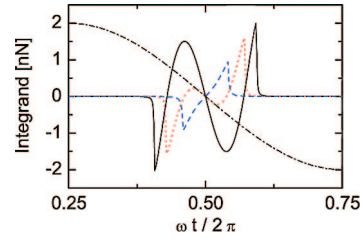

Figure 8. Time dependence of the integrand in eq 11 during an oscillation for the same parameters as in Figures 6 and 7. For comparison, the time dependence of a sine function in the integrand is also shown as a dash-dotted line.

of a short and high pulse at $\omega t = \pi$. This pulse results in a positive value for k_{ts}, which shifts the resonance frequency ω_0 to higher values and decreases the amplitude a such that it matches the distance z_0. This solution corresponds to a point on the left flank of the resonance curve in Figure 2.

Applicability of Harmonic Models. We now turn to the question under which conditions it is justified to describe the cantilever dynamics in the harmonic approximation. The typical damping of an oscillating cantilever in air is low, and correspondingly the quality factor Q is high ($Q \approx 500$). Even during intermittent contact with the sample for typical imaging conditions Q stays above 200. Such a resonant system with a high quality factor behaves like a filter which strongly limits excitations at higher harmonics of the fundamental (typically below 1% of the amplitude).[24,25] This allows to construct a meaningful harmonic solution of eq 3, even if F_{ts} depends in a nonlinear way on z. Correspondingly, the lock-in amplifier in an atomic force microscope usually only measures the parameters of the first harmonic. Higher harmonics may not be negligible if they coincide with higher eigenmodes of the cantilever structure.[26] Also, for imaging in liquids with the typical small quality factors below 10 the applicability of harmonic models may be limited. The harmonic approximation was tested experimentally; Bar et al. show exemplary measurements for PDMS and PS surfaces.[27] Not only the typical shape of $a(\omega)$ and $\varphi(\omega)$ was verified but also the shift of resonance frequency and damping during the approach to the surface. Numerical simulations also showed that for the typical conditions of imaging in intermittent contact only small perturbations of the resonance curves show up.[17,28] A direct comparison of these results with eqs 13 and 14 is difficult, as during a frequency scan at a fixed zero position of the cantilever the effective interaction with the surface changes due to the changing oscillation amplitude; i.e., parameters ω_0 and Q are not constant. The same applies for numerical calculations.[28,29] San Paulo and Garcia[28] showed explicitly how for a fixed distance of the cantilever from a hard surface the resonance curve gets heavily distorted for oscillation amplitudes larger than the distance. With increasing excitation amplitude the maximum of the resonance curve first slightly shifts toward smaller frequencies, and then, with the repulsive interaction becoming

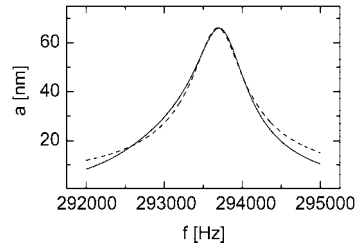

Figure 9. Free resonance curve of cantilever 1 (solid line) and corresponding model curve according to eq 13 (dashed line, parameters are given in Table 1).

stronger it shifts toward higher frequencies, as discussed above. Of course, this does not mean that the sinusoidal form of the oscillation itself gets disturbed.

Calculation of Interaction Parameters from Measured Data. Given that an adequate physical description of the tip−sample interaction can be achieved with the parameters k_{ts} and α_{ts}, the question arises if these parameters can be determined from the parameters amplitude and phase accessible in the experiment. Under the assumption that eqs 13 and 14 are valid during intermittent contact, the parameters ω_0 and Q will change accordingly. Inverting eqs 13 and 14 separates conservative and dissipative effects.

$$\frac{k + k_{ts}}{m} = \frac{k_{eff}}{m} = {\omega_0}^2 = \omega^2 + \cos(\varphi)\frac{F_0/m}{a} \tag{19}$$

$$\alpha_{eff}/m = \frac{\omega_0}{Q} = \frac{-\sin(\varphi)}{\omega}\frac{F_0/m}{a} \tag{20}$$

For an overview we want to discuss how the parameters k_{eff} and α_{eff} suggested here for the analysis of AFM measurements are related to other parameters used in the literature to analyze the tip−sample interaction, namely the mean dissipated power $\langle P_{tip}\rangle$ and the mean interaction force $\langle F_{ts}\rangle$. For high-quality factors and negligible internal damping of the cantilever compared to the external hydrodynamic damping the following expression holds:[24]

$$\langle P_{tip}\rangle = \langle P_{in}\rangle - \langle P_{diss,free}\rangle = \frac{\omega a}{2}[k a_d \sin\varphi - \alpha a\omega] \tag{21}$$

Here $\langle P_{in}\rangle$ is the power put into the system by the driver and $\langle P_{diss,\,free}\rangle$ is the power dissipated by the free cantilever through hydrodynamic damping. a_d is the oscillation amplitude of the dither driving the base of the cantilever. $\langle P_{tip}\rangle$ can also be expressed as

$$\langle P_{tip}\rangle = \frac{1}{2}\frac{\omega a^2 k}{Q_{free}}\left[\frac{Q_{free}a_d}{a}\sin\varphi - \frac{\omega}{\omega_{0,free}}\right] \tag{22}$$

where Q_{free} is the quality factor of the free cantilever without interaction to the sample and $\omega_{0,\,free}$ is the resonance frequency of the free oscillating cantilever. This result is consistent with the description by the tip−sample interaction parameters discussed above. Under stationary conditions the total dissipated power $\langle P_{diss,\,tot}\rangle$ is equal to the power $\langle P_{in}\rangle$ introduced by the driver, and using eq 20 $\langle P_{tip}\rangle$ is obtained as

$$\langle P_{tip}\rangle = -\langle P_{diss,tot}\rangle - \langle P_{diss,free}\rangle \tag{23}$$

$$= -\frac{1}{2}a^2\omega^2\alpha_{eff} - \frac{1}{2}a^2\omega^2\alpha \tag{24}$$

$$= \frac{\omega a}{2}(k a_d \sin\varphi - a\omega\alpha) \tag{25}$$

Here we used $F_0 = k a_d$. The mean power $\langle P_{tip}\rangle$ has been used for instance to interpret force spectroscopy curves. Because of its strong dependence on amplitude, it has also been suggested to use alternatively a relative measure by normalizing $\langle P_{tip}\rangle$ to the kinetic energy of the oscillation.[30] The dissipated energy $\langle P_{tip}\rangle$ emphasizes the aspect of dissipation in the interaction of tip and sample.

Another parameter suggested in the literature[18] for the interpretation of the interaction of tip and sample is the mean value of the interaction force $\langle F_{ts}\rangle$. It is determined by application of the virial theorem[31]

$$\frac{1}{2}m\langle \dot{z}^2\rangle = -\frac{1}{2}\langle F\cdot z\rangle \tag{26}$$

to eq 1. Under the harmonic assumption and for excitation at the natural frequency of the free cantilever one gets approximately[18]

$$\cos\varphi \approx -\frac{2Q\langle F_{ts}\cdot z\rangle}{k a a_0} \tag{27}$$

where a_0 is the amplitude of the free cantilever. Under the assumption of negligible tip−sample power dissipation and small contact times this leads to[18]

$$\cos\varphi \approx 2\frac{\langle F_{ts}\rangle}{F_0} \tag{28}$$

which shows that the cosine of the phase angle is a direct measure of the mean force on the tip under these conditions. The result in eq 27 can also be obtained from the parameters of the harmonic model outlined above. Starting from eq 19, we get

$$\cos\varphi = \frac{a}{F_0}(k + k_{ts} - \omega^2 m) \tag{29}$$

If ω is equal to the resonance frequency of the free cantilever, $m\omega^2 = k$. Using eq 12, we obtain eq 27

$$\cos\varphi = \frac{a}{F_0}k_{ts} = \frac{a}{k a_d}\left(-\frac{2}{a^2}\langle F_{ts}\cdot z\rangle\right) = -\frac{2Q}{k a_0 a}\langle F_{ts}\cdot z\rangle \tag{30}$$

One notices that the average $\langle F_{ts}\cdot z\rangle$ isolates the elastic contributions of the tip−sample interaction. However, from eqs 21 and 27 as well as eqs 19 and 20 it becomes apparent that a change in phase angle φ corresponds to a simultaneous change in conservative and dissipative part of the interaction. A full record of the tip−sample interaction requires the determination of both contributions.

Experimental Section

AFM. All measurements were done with a commercial atomic force microscope Nanowizard from JPK Instruments (Berlin, Germany). Two types of silicon cantilevers from Nanoworld with a nominal resonance frequency of 320 kHz and a stiffness of about 42 N/m or a resonance frequency of 75 kHz and a stiffness of 1.3 N/m were used. Most of the measurements shown here were performed with an excitation frequency $\omega = 0.9995\omega_0$. The resonance curve of the freely oscillating cantilever was measured before data acquisition. A fit according to eq 13 gave the parameters of the cantilever (Figure 9). They are given in Table 1 for the cantilevers used here. In the range of the resonance peak the model function describes the data reasonably well.

Sample. Spin-coated films of polystyrene (PS) and cross-linked polydimethylsiloxane (PDMS, Sylgard 184) were used as model surfaces for force spectroscopy. PS at room temperature is a hard glassy material with a shear modulus of about 2 GPa. Mechanical dissipation is very weak. For the PDMS sample mechanical

Table 1. Oscillation Parameters of the Cantilevers Used[a]

cantilever	k [N/m]	ω_0 [rad/s]	F_0/m [m/s^2]	Q	$m = k/\omega_0^2$ [kg]
1	42	1.8453×10^6	469.03	488	12.33×10^{-12}
2	1.295	3.5368×10^5	58.89	130	11.03×10^{-12}

[a] The values for the force constant k were either given by the supplier (cantilever 1) or measured by analyzing the thermal excitation spectrum of the cantilever (cantilever 2). All other parameters were determined from the resonance curve of the free cantilevers.

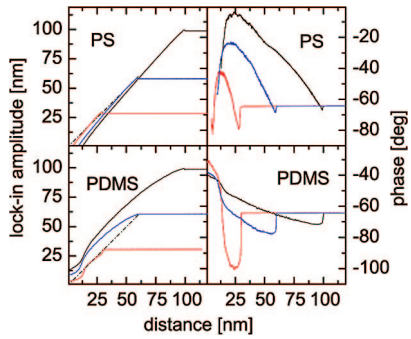

Figure 10. Force spectroscopy curves on model surfaces of PS and PDMS for different free amplitudes of 30, 60, and 100 nm with the stiff cantilever 1 and an excitation frequency of $0.9995\omega_0$. The dash-dotted line in both amplitude diagrams would correspond to an amplitude equal to the distance from the surface.

measurements for a series of temperatures and frequencies in the range of 0.01−100 rad/s were performed on bulk samples. Even after extrapolation to the measurement frequency of the AFM using time−temperature superposition[32] the main relaxation zone of PDMS is below room temperature, and the extrapolated value of the modulus is about 1.5 decades smaller than for PS. Accordingly, for the AFM measurements PDMS behaves like a soft material without strong dissipation.

For imaging experiments semicrystalline polyethylene (LDPE, obtained from Aldrich) was used. Polyethylene consists of stacks of alternating crystalline and amorphous layers with typical thickness in the 10 nm range. Since the glass transition temperature of amorphous PE lies well below room temperature, the material shows a strong hard−soft contrast in the AFM. The samples were hot-pressed between glass plates. After removal of one of the plates the sample was heated above the melting temperature and slowly cooled. Subsequently, the free surface was investigated in the AFM.

Force Spectroscopy on Model Surfaces

Hard and Soft Model Surfaces in Comparison. In so-called force spectroscopic measurements amplitude and phase shift of the oscillating cantilever are measured at a fixed lateral position while varying the distance to the surface of the sample. Frequency and amplitude of the excitation are kept constant. Figure 10 shows exemplary data measured with the stiff cantilever 1 and free amplitudes of 30, 60, and 100 nm on PS and PDMS. In the experiments the zero point for the distance to the surface is not measured on an absolute scale; it was adjusted such that the first effects of interaction in the curves show up at a distance corresponding to the free amplitude.

PS shows the typical behavior of a hard surface: the amplitude decreases approximately linear with the distance to the surface, and the phase shift shows over a large range of distances increasing values, usually interpreted as being caused by repulsive interactions. In contrast, for PDMS the amplitude decreases in a nonlinear way and less steeply which indicates that the cantilever indents into the surface.[33,34] The phase shift shows lower values than the free oscillating cantilever over a large range of amplitudes. As discussed above, amplitude and phase depend on the interaction through k_{eff} and α_{eff} as described by eqs 13 and 14. By using the harmonic model of eqs 19 and

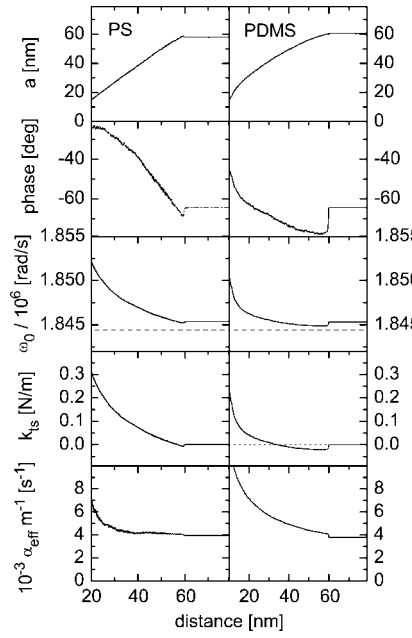

Figure 11. Force spectroscopy on PS and PDMS surfaces: oscillation amplitude a, phase shift φ, resonance frequency ω_0, effective tip−sample force gradient k_{ts}, and damping constant α_{eff}/m vs distance. The excitation frequency was $0.9995\omega_0$ of the free cantilever and the free amplitude 60 nm in both cases. The dashed horizontal line gives the excitation frequency for comparison; the spring constant of the free cantilever was 42 N/m.

20 one can transform the data into the momentary resonance frequency ω_0 or interaction parameters k_{ts} and α_{eff}. This analysis separates conservative and dissipative contributions of the interactions and allows a straightforward interpretation of the data. To do so, one has to fix the origin of the measured phase scale such that the phase of the free cantilever at resonance is −90°. Usually, during experiments the phase is set arbitrarily to zero at a distance of some micrometers to the sample surface. From the known parameters of the free resonance curve one can calculate the value of the phase shift for the chosen excitation frequency. For all data shown below the measured phase values were shifted to bring them to this value for large tip−sample distances. The results of such an analysis are summarized in Figure 11 for PS and PDMS, based on the data set with a free amplitude of 60 nm. The top panel in Figure 11 shows again the amplitude for comparison. The next panel gives the phase shift, already adjusted to the value of −64.3° at large distance as calculated for an excitation frequency of $0.9995\omega_0$. Underneath the resonance frequency ω_0 in dependence on the distance to the surface is shown. The dashed line shows the excitation frequency for comparison. The interaction parameter for the conservative interaction k_{ts} is plotted in the next panel. The lowest panel in Figure 11 shows the effective damping of the whole system α_{eff}.

Figure 11 enables an unambiguous interpretation of the data. Before comparing PS and PDMS in detail, we consider the general effects of the interaction between tip and sample, which show up qualitatively for both samples. We concentrate on the part of the curves not too close to the sample surface because for the latter region the harmonic models may become inapplicable, and there are larger uncertainties in phase shift values due to technical reasons. On approaching the surface from a state of free oscillation the tip will first feel the attractive forces before it touches the surface. According to eq 10, these forces cause a negative contribution to k_{eff} and lower the resonance frequency accordingly. For an excitation frequency below resonance, lowering the resonance frequency causes an increase

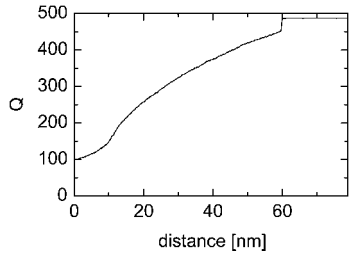

Figure 12. Calculated dependence of quality factor Q of the whole oscillating system on distance to the sample surface for the poly(dimethylsiloxane) sample for the same measurement parameters as in Figure 10.

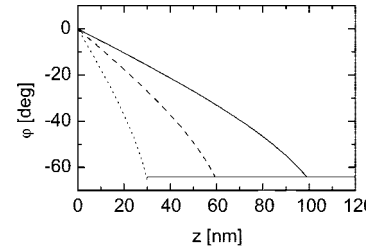

Figure 13. Calculated dependence of phase shift φ on the tip−sample distance z for an infinitely hard surface without additional dissipation and different free amplitudes (30, 60, and 100 nm). The horizontal line marks the phase shift for the first contact with the surface, for an excitation frequency $\omega = 0.9995\omega_{0,\,\mathrm{free}}$.

in amplitude (if we suppose for the moment no additional damping). If the amplitude increases for a fixed distance from the surface, the tip will sense the attractive force for a longer time during each oscillation cycle, and this in turn will increase the effect even further. This self-amplification effect causes the sudden decrease of the phase shift when the tip first feels the surface. In the amplitude signal the corresponding effect is only small and harder to see. With the first direct contact of tip and surface repulsive forces come into play and stop the increase in amplitude because their positive contribution to k_{ts} stops the decrease in the resonance frequency. This happens for both samples well before the resonance frequency reaches the excitation frequency because an excitation frequency far enough below the resonance frequency was used. So the system stays on the left side of the resonance peak. Upon further approach repulsive interactions increase, and the resonance peak moves to the right. The amplitude decreases accordingly. This effect is self-stabilizing which causes the smooth dependence of amplitude and phase shift on distance. Note that at this point the linearity of k_{ts} in the forces (cf. eq 10) is essential; k_{ts} results from an additive superposition of attractive and repulsive force contributions. Also, the effective tip−sample force gradient k_{ts} remains always small compared to the stiffness k of the cantilever. This justifies the treatment of the tip−sample interaction as a small perturbation. The additional damping due to tip sample interaction can be relatively strong as the example of PDMS shows. Nevertheless, the corresponding quality factor, which is shown in Figure 12, remains in the range of some hundreds. These are conditions which still allow the application of the harmonic model.

On the basis of this general scenario, the different interactions of the tip with the two surfaces, PS and PDMS respectively, are easily rationalized. In short, PS acts as a hard surface, for which even very small deformations give rise to large repulsive forces. The amount of damping due to contact with the surface is limited. PDMS on the other hand is a much softer material. Appreciable repulsive forces require large deformations. As mentioned above, the different shape of the amplitude vs distance curves indicates much stronger indentation and therefore deformation of the surface in case of PDMS. Nevertheless, the net value of k_{ts} remains negative for about the first 25 nm of approach. The attractive interaction, although it will be of similar magnitude as for PS, dominates since the repulsive contribution is so small in the case of PDMS. This leads to the large range with negative phase shift and lower resonance frequency. Only for hard tapping conditions the increasing repulsive contributions[35] will cause a positive k_{ts}. For PS, on the other hand, the repulsive forces are strong and dominate, which makes the range of distances with a negative phase shift very small. Damping effects are also much larger in case of PDMS, and the approximately parallel increase in k_{ts} and α_{eff}/m with decreasing distance indicates that damping is also related to deformation of the sample. In comparison for PS over most of the distance range the decrease in amplitude is dominantly caused by elastic repulsive forces and the corresponding shift in resonance frequency, while for PDMS damping is an important factor and the shift in resonance frequency is smaller.

Note that all values of force gradient k_{ts}, damping parameter α_{ts}, and quality factor Q are not direct material properties of the sample. They also depend on the type of contact and deformation, i.e., tip geometry and indentation depth.

Variation of the Free Amplitude. From the measurements shown in Figure 10 it appears that with decreasing free amplitude the effect of attractive interactions showing up in negative phase shift gets more pronounced. This effect can be qualitatively understood in a simple way. The prefactor of the integral over the force which determines k_{ts} (cf. eq 10) is proportional to $1/a$, in addition the tip is in reach of the attractive interaction over a larger fraction of the period of the oscillation. Both factors contribute to a stronger effect of the attractive interactions for smaller free amplitudes. For the case of a soft material and a small amplitude the sample might not develop enough repulsive forces to limit the increasing amplitude on the left flank of the resonance curve. Then, because of the interaction, the resonance frequency falls below the excitation frequency and the system finds itself on the right-hand side of the resonance peak. This causes phase values below −90° and steeply decreasing amplitudes at the onset of interaction as visible in Figure 10 for 30 nm free amplitude on PDMS.

On the other hand, as is visible for PS, in the range of dominantly repulsive interaction the slope of the phase−distance curve is larger for small amplitudes. The way how k_{ts} in general depends on the oscillation amplitude is not so obvious, since in this case also the amplitude of the force F_{ts} in eq 10 can change with the oscillation amplitude. A simple model can be formulated for the approximation of an infinitely hard surface without attractive and dissipative interaction. If the dissipation of the cantilever is constant and the amplitude equal to the distance from the surface, one can calculate the phase shift φ from eq 20 as

$$\varphi = -\arcsin\left(\frac{\omega\alpha_{\mathrm{eff}}}{F_0}a\right) \approx -\arcsin\left(\frac{\omega\alpha_{\mathrm{eff}}}{F_0}z\right) \qquad (31)$$

Figure 13 shows that this simple model closely resembles the trends in the measured phase shift data for PS in the repulsive regime in Figure 10.

Variation of Excitation Frequency. Figure 14 shows the influence of the excitation frequency on the force spectroscopy curves. For PS one finds the classical behavior of a sample without much additional dissipation.[1] Upon approaching the surface, first in the attractive regime the phase decreases. This is accompanied by an increase in amplitude if the excitation frequency is smaller than the resonance frequency ω_0 of the free cantilever. For an excitation at or above ω_0 an increase of attractive forces and a corresponding shift of the resonance

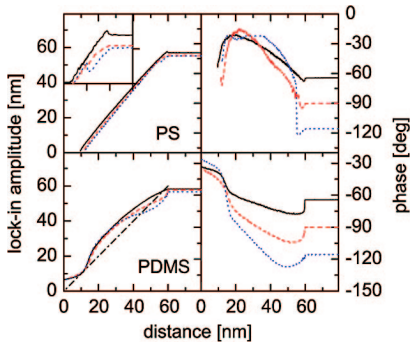

Figure 14. Influence of excitation frequency on spectroscopy curves for PS and PDMS with the stiff cantilever 1 and free oscillation amplitude of 60 nm. The solid, dashed, and dotted lines correspond to an excitation frequency of 0.9995, 1.0000, and 1.0005 times the free resonance frequency. The inset shows for PS a zoom into the amplitude curves over a distance range from 50 to 65 nm. The dash-dotted line gives a slope of one for comparison.

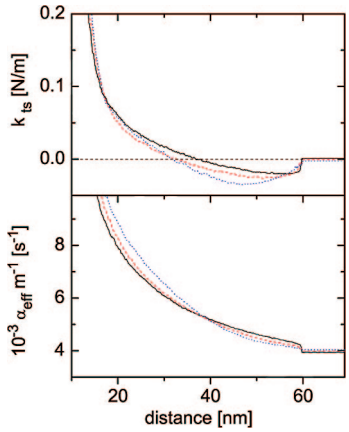

Figure 15. Comparison of the calculated interaction parameters from spectroscopy curves for PDMS with the stiff cantilever 1 for different excitation frequencies. The solid, dashed, and dotted lines correspond to an excitation frequency of 0.9995, 1.0000, and 1.0005 times the free resonance frequency.

frequency to lower values can only decrease the amplitude. This decrease in amplitude is self-stabilizing. Hence, while approaching the surface under these conditions, the phase angle decreases continuously and not suddenly. Later during the approach the system leaves the attractive regime and jumps to the repulsive regime, signaled by the large positive jump in phase shift and a small jump in amplitude.

For PDMS one finds, especially in the amplitude data, many more details which can be interpreted by our approach. Figure 15 shows k_{ts} and α_{eff}, calculated from the data of Figure 14 according to our eqs 19 and 20. The negative values of k_{ts} while approaching the surface indicate the range of dominating attractive forces. Their effect is strongest for excitation above the resonance frequency because there any decrease in resonance frequency also decreases the amplitude. This shows up as the steep decrease in amplitude in Figure 14 for PDMS and excitation at 1.0005 of the resonance frequency. The tip does not penetrate the sample surface because the attractive forces alone can reduce the amplitude according to the reduced distance. Going from 1.0005 over 1.0000 to 0.9995 times resonance frequency of the free cantilever for instance at around 50 nm distance, one notices in the case of PDMS an increase in surface penetration in Figure 14 and growing repulsive and damping contributions in Figure 15. Working on the left-hand side of the resonance peak emphasizes the repulsive contributions because a decrease in amplitude can only be achieved here

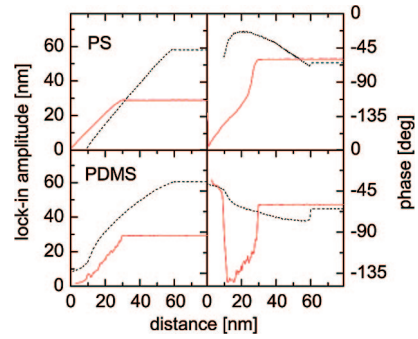

Figure 16. Influence of spring constant k of the cantilevers (cantilever 1: 42 N/m (dashed line); cantilever 2: 1.3 N/m (solid line)) on force spectroscopy curves on PS and PDMS. The excitation frequency was 0.9995 of the resonance frequency of the free cantilever and the free amplitude far from the surface 60 and 30 nm, respectively.

by a shift in resonance frequency to higher values (or an increase in damping, which is also connected to repulsive forces from indentation in our case). Below about 40 nm distance for PDMS the repulsive forces dominate. k_{ts} in Figure 15 becomes positive, and in Figure 14 one finds penetration of the surface in all cases; i.e., all amplitudes are lying above the dash-dotted line.

Variation of the Cantilever Stiffness. For the stiff cantilever we discussed that the attractive forces are in most cases not strong enough to shift the resonance frequency below the excitation frequency. The system always stays on the left side of the resonance peak. The situation can be completely different for a softer cantilever. The reason is that for a given effective tip−sample force gradient k_{ts} the shift of the resonance curve is larger for a softer cantilever, i.e., smaller k. This shift can easily be calculated from eq 15.

$$\frac{\omega_0(k_{ts})}{\omega_0(k_{ts}=0)} = \sqrt{\frac{(k+k_{ts})/m}{k/m}} = \sqrt{1+\frac{k_{ts}}{k}} \approx 1+\frac{1}{2}\frac{k_{ts}}{k} \tag{32}$$

Figure 16 shows exemplary force spectroscopy data for a stiff (1) and a soft (2) cantilever on PS and PDMS in comparison. For the soft cantilever a smaller free amplitude a of 30 nm was used to emphasize the attractive contributions (see eq 10). Obviously, the curves for the two cantilevers look completely different. It is interesting to note that, in contrast to the results presented above, both surfaces look rather similar if measured with the soft cantilever.

The interaction parameters of the stiff cantilever were already discussed above. We here concentrate on the analysis of the case of the soft cantilever 2. Figure 17 shows the effective interaction parameters vs distance. For the soft cantilever on both surfaces the resonance frequency decreases at the beginning of interaction below the excitation frequency because of the strong effect of the attractive forces. There is a remarkable similarity between the interaction parameters from both surfaces over a large range of distances. For about half the range k_{ts} is negative and nearly the same for both surfaces. This is expected if the attractive interactions dominate. For even closer contact of tip and sample the damping strongly increases (cf. Figure 17). This leads to low values of the quality factor around 30, and the harmonic model may be not numerically adequate there. Without going into further detail here, it is important to realize that the value of the cantilever stiffness has a large effect on the nature of the measured interaction forces between cantilever and surface. Furthermore, the use of soft cantilevers originally designed for contact mode operation may open the possibility to easily perform AFM measurements in the attractive mode in

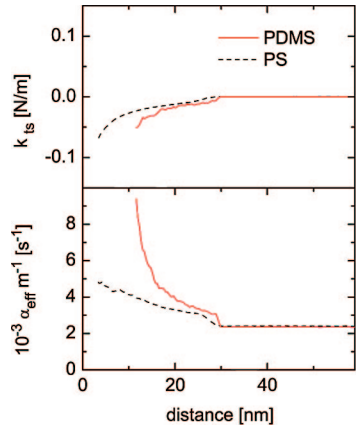

Figure 17. Interaction parameters for the measurement with the soft cantilever as calculated from force spectroscopy data shown in Figure 16.

a well-controlled way. This issue will be further explored in future work.

Interpretation of Images in Intermittent Contact Mode

Discussion of Simplified Cases. Let us now try to use the results above for the interpretation of contrast in imaging. As already mentioned, in intermittent contact (AM) mode the feedback system of the AFM keeps the amplitude $a(\omega)$ constant by adjusting the height of the tip while scanning the sample. It follows from eqs 19 and 20 that during scanning due to the constant amplitude a change in phase always indicates a change in both interaction constants according to the following relations:

$$k_{ts} \sim c_1 + c_2 \cos(\varphi) \tag{33}$$

$$\alpha_{eff} \sim c_3(-\sin(\varphi)) \tag{34}$$

It should be kept in mind that k_{ts} and α_{eff} depend on the properties of the underlying substrate and the height of the tip above the sample.

Let us first discuss the nature of image contrast for some idealized cases of flat surfaces without topography but with patterns of contrast in either conservative or dissipative forces only. First we consider a hypothetical surface with a contrast in conservative interaction without any dissipative tip−sample interaction. According to eq 34, the constant, height-independent dissipation of the bare cantilever results in a constant phase shift. Therefore, in order to keep $a(\omega)$ constant, the feedback loop will change the height z of the tip to keep the effective force gradient k_{ts} constant (eq 33). This obviously results in artifacts in the topography image. This conclusion is in line with the general statement that there is no phase contrast in imaging without dissipation contrast.[36]

As a second case we consider another hypothetical flat surface with material contrast in dissipation but constant, height-independent conservative forces. The latter results according to eq 33 again in a constant phase shift. The feedback loop will now change the height to keep the effective damping constant (eq 34). This again results in topographical artifacts without phase contrast. According to eq 22, also the dissipated energy is constant. In this case the contrast in material dissipation does not show up in phase shift or dissipated energy. It is masked by the feedback loop trying to keep the amplitude constant. In practical cases of course both dissipation and conservative forces are present and possible sources of phase contrast. And indeed, a necessary condition for phase contrast to occur is that both conservative and dissipative interactions are present and that both depend on the tip−sample distance.

To illustrate this more realistic case, we finally discuss image contrast for a hypothetical flat model surface consisting of patches of PS and PDMS with the properties measured above. There is contrast in conservative forces resulting from different repulsive contributions as well as stronger damping connected with deformation in PDMS. We assume the AFM works with an excitation frequency below the resonance frequency; accordingly, the phase shift will be above −90°. On the hard surface (PS) the dominantly repulsive interaction leads to an upward shift of the resonance frequency; the oscillating system is mistuned and the amplitude reduced. In this way the required amplitude (set point) can be realized by adjusting the height z of the tip. If the tip enters the region with the smaller repulsive interactions (PDMS) the resonance frequency of the cantilever will decrease, and accordingly the amplitude will increase and the phase decrease. The feedback loop for the amplitude will now try to hold a constant by varying the height of the tip. In case of PDMS Figure 11 shows that over a large range of distances the conservative forces and accordingly the resonance frequency of the cantilever depend only slightly on the height of the tip, whereas the damping is affected more strongly. The feedback system will increase dissipation (and to a minor extent repulsive interaction) by lowering the height. Mostly due to the increasing dissipation the amplitude will become smaller again while still fulfilling eqs 33 and 34. So in this case there exists a phase contrast accompanied by an artificial height signal due to stronger indentation on the soft parts of the sample. This contrast in dissipation or α_{eff} is not caused by direct material dissipation contrast but by a change in interaction strength due to a changing height of the tip, which in turn was induced by changing conservative forces. This specific example illustrates the general fact that α_{eff} or the dissipated energy is not directly a material property but a measure of the interaction strength under the given conditions of the oscillation.

Exemplary Measurements on a Semicrystalline Polymer with Hard−Soft Contrast. AFM measurements in intermittent contact mode are a routine method for the analysis of heterogeneous polymer systems carrying structure on the nanoscale. The underlying contrast is normally related to the different mechanical properties of the components. Even if today a quantitative measurement of local mechanical properties is normally out of reach, an improved and simple understanding of the image parameters can be helpful in order to identify different components in the image and to gain qualitative information about local mechanical properties.

Figure 18 shows as a practical example a height and a phase image of a semicrystalline sample of polyethylene. The stripe pattern obviously shows the semicrystalline morphology of the sample consisting of lamellar crystals and amorphous layers in between. A scan showing the values of the two parameters along the line indicated in the images is given in the upper panel of Figure 19. For a more detailed discussion it is useful again to calculate interaction parameters from the measured quantities. Again, the measured value of the phase has to be set to an absolute scale as already described above for the force spectroscopic measurements. k_{ts} and α_{eff} can then be calculated with eqs 19 and 20. The two lower panels of Figure 19 show the results of this calculation for the line scan indicated in Figure 18. As an example, let us focus on the position marked by the vertical dotted line in Figure 19. There the damping is comparatively low and the repulsive contributions in k_{ts} are high. From the comparison with the results on the model surfaces one would infer that the surface is comparatively hard at this position. This is compatible with the peak in the height signal at this position. As discussed above, the height signal does not necessarily show the real topography of the surface but a combination of real topography and of indentation, which is

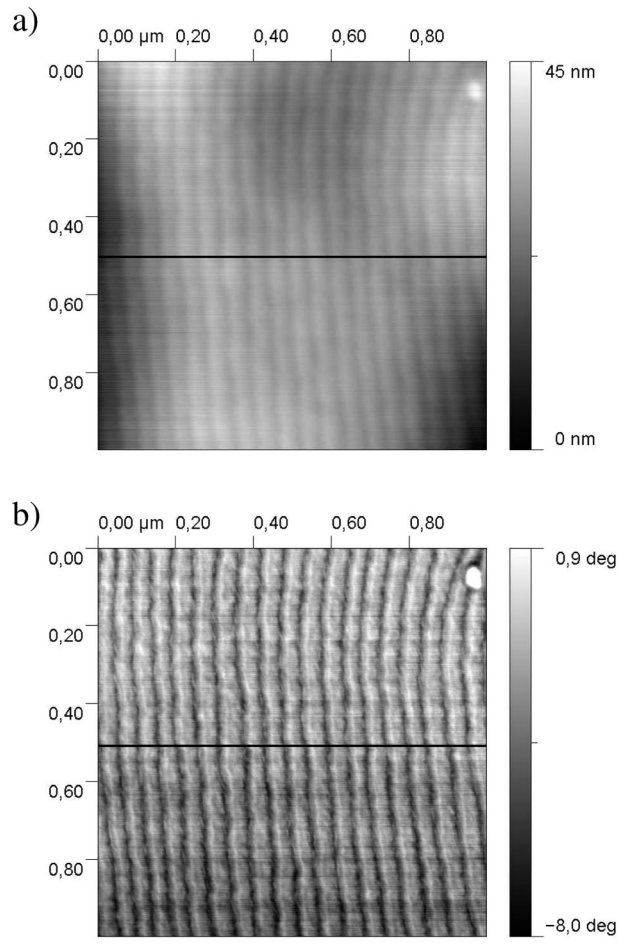

Figure 18. Height (a) and phase images (b) (raw data) of the surface of a semicrystalline sample of polyethylene (set point $r = 0.9$, amplitude $a = 60$ nm, $\omega/\omega_0 = 0.9995$). The line scan further analyzed below is indicated by the horizontal line.

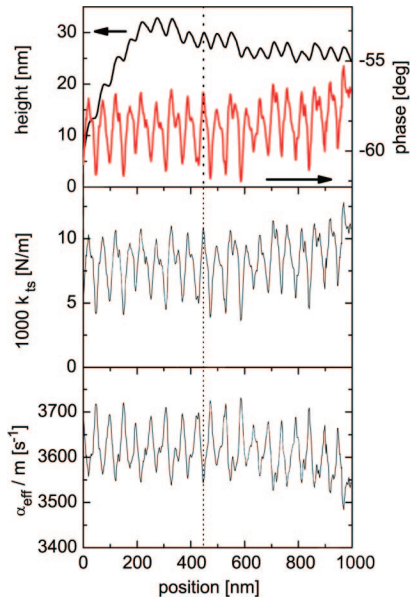

Figure 19. Height, phase, effective tip−sample force gradient, and effective damping for the line scan on the partially crystalline sample of polyethylene, calculated from the data of Figure 18.

smaller on the hard crystalline component. These findings all together allow to conclude unambiguously that the marked position corresponds to a crystalline lamellae. In between those lamellae are the softer amorphous regions, which in the original

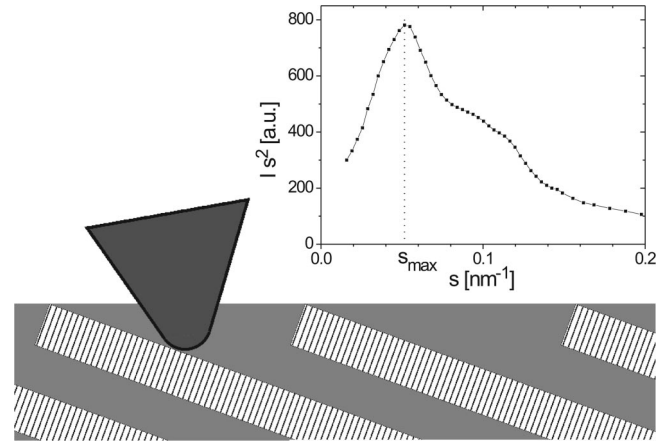

Figure 20. Schematic model for the lamellar structure of the sample shown in Figure 18 and its interaction with the AFM tip. The inset shows the result of a SAXS measurement ($I(s)s^2$ vs s) with the peak position corresponding to the inverse long period ($s_{max} = 0.052$ nm^{-1}).

image show a lower value of the phase. It should not be overlooked though that the variations in k_{ts} and α_{eff} are considerably smaller than for the model surfaces measured by force spectroscopy and that k_{ts} is positive on both parts of the sample. Also, the apparent mean repeat distance of the lamellae is about 53 nm, considerably larger than the long period $L \simeq 19$ nm, as determined from small-angle X-ray scattering (SAXS) on the same sample (inset in Figure 20). The difference can be rationalized by the schematic model shown in Figure 20. The larger lateral repeat distance of the lamellae in the AFM picture is a result of the inclination of the lamellae with respect to the surface of the sample. The values mentioned correspond to an angle of about 20° between the normals of the sample surface and the lamellae. Because of this small angle, the tip hits the interlamellar layer in a direction close to lamellar normal. Figure 20 illustrates that the AFM tip due to its finite size and due to the finite thickness of the interlamellar material will interact not only with amorphous but also with the crystalline material. Hence, the sample properties sensed by the tip will correspond to an average over crystalline and amorphous regions, and the contrast is indeed expected to be much smaller than the difference between pure crystalline and amorphous model surfaces. This is also consistent with the small experimental value of the phase contrast between lamellar and interlamellar domains, which is much smaller than for the soft and hard model substrates in Figure 11.

Conclusions

Under typical ambient imaging conditions the small damping or correspondingly the high-quality factor of the AFM cantilever allows the successful application of relatively simple harmonic models for a qualitative and quantitative interpretation of AFM data in intermittent contact mode. These models permit a separation of conservative and dissipative contributions of the tip−sample interaction if the parameters of the resonance curve for the free oscillating cantilever and the origin of the phase shift scale are known. The separate experimental determination of both contributions improves the qualitative understanding of image contrast and the possibilities for a comparison of AFM data to theoretical interaction models. From a technical point of view the approach presented here enables a well-formulated understanding of the influence of measurement parameters like cantilever stiffness, oscillation amplitude or set point, excitation frequency, etc., on measurement or imaging process. We believe that the effective force gradient and the effective dissipation

could also serve as a suitable starting point for a comparison with detailed simulations of tip−sample interaction.

Acknowledgment. We thank the German Science Foundation and State Sachsen-Anhalt for financial support.

References and Notes

(1) *Applied Scanning Probe Microscopy*; Bhushan, B., Fuchs, H., Hosaka, S., Eds.; Springer: Berlin, 2004.
(2) Sheiko, S. S. *Adv. Polym. Sci.* **2000**, *151*, 61.
(3) Hofer, W. A.; Foster, A. S.; Shluger, A. L. *Rev. Mod. Phys.* **2003**, *75*, 1287.
(4) Giessibl, F. J. *Rev. Mod. Phys.* **2003**, *75*, 949.
(5) García, R.; Pérez, R. *Surf. Sci. Rep.* **2002**, *47*, 197.
(6) Bar, G.; Delineau, L.; Brandsch, R.; Bruch, M.; Whangbo, M. H. *Appl. Phys. Lett.* **1999**, *75*, 4198.
(7) Godehardt, R.; Lebek, W.; Adhikari, R.; Rosenthal, M.; Martin, C.; Frangov, S.; Michler, G. H. *Eur. Polym. J.* **2004**, *40*, 917.
(8) Bar, G.; Thomann, Y.; Brandsch, R.; Cantow, H. J.; Whangbo, M. H. *Langmuir* **1997**, *13*, 3807.
(9) Garcia, R.; Gómez, C. J.; Martinez, N. F.; Patil, S.; Dietz, C.; Magerle, R. *Phys. Rev. Lett.* **2006**, *97*, 016103.
(10) Lee, M. H.; Jhe, W. H. *Phys. Rev. Lett.* **2006**, *97*, 036104.
(11) García, R.; Magerle, R.; Perez, R. *Nat. Mater.* **2007**, *6*, 405.
(12) Hölscher, H. *Appl. Phys. Lett.* **2006**, *89*, 123109.
(13) Leclère, P.; Viville, P.; Jeusette, M.; Aimé, J.-P.; Lazzaroni, R. Scanning Probe Microscopy of Complex Polymer Systems: Beyond Imaging their Morphology. In *Scanning Probe Microscopies Beyond Imaging*; Samori, P., Ed.; Wiley-VCH: New York, 2006; Chapter 7, p 175.
(14) Schirmeisen, A.; Hölscher, H.; Anczykowski, B.; Weiner, D.; Schäfer, M. M.; Fuchs, H. *Nanotechnology* **2005**, *16*, S13.
(15) Hölscher, H.; Anczykowski, B. *Surf. Sci.* **2005**, *579*, 21.
(16) Hu, S.; Raman, A. *Nanotechnology* **2008**, *19*, 375704.
(17) Paulo, A. S.; García, R. *Surf. Sci.* **2001**, *471*, 71.
(18) Paulo, A. S.; García, R. *Phys. Rev. B: Condens. Matter Mater. Phys.* **2001**, *64*, 193411.
(19) Rodríguez, T. R.; García, R. *Appl. Phys. Lett.* **2002**, *80*, 1646.
(20) Rabe, U.; Hirsekorn, S.; Reinstädtler, M.; Sulzbach, T.; Lehrer, C.; Arnold, W. *Nanotechnology* **2007**, *18*, 044008.
(21) Herruzo, E. T.; Garcia, R. *Appl. Phys. Lett.* **2007**, *91*, 143113.
(22) Attard, P. *J. Phys.: Condens. Matter* **2007**, *19*, 473201.
(23) Hölscher, H.; Ebeling, D.; Schwarz, U. D. *J. Appl. Phys.* **2006**, *99*, 084311.
(24) Cleveland, J. P.; Anczykowski, B.; Schmid, A. E.; Elings, V. B. *Appl. Phys. Lett.* **1998**, *72*, 2613.
(25) Sebastian, A.; Salapaka, M. V.; Chen, D. J.; Cleveland, J. P. *J. Appl. Phys.* **2001**, *89*, 6473.
(26) Wang, W. L.; Hu, S. J. *Appl. Phys. Lett.* **2005**, *87*, 183506.
(27) Bar, G.; Brandsch, R.; Whangbo, M. H. *Langmuir* **1998**, *14*, 7343.
(28) Paulo, A. S.; García, R. *Phys. Rev. B: Condens. Matter Mater. Phys.* **2002**, *66*, 041406.
(29) Sasaki, N.; Tsukada, M. *Jpn. J. Appl. Phys., Part 2* **1998**, *37*, L533.
(30) Bar, G.; Brandsch, R.; Bruch, M.; Delineau, L.; Whangbo, M. H. *Surf. Sci.* **2000**, *444*, L11.
(31) Goldstein, H. *Klassische Mechanik*; AULA-Verlag: Wiesbaden, 1991; p 76.
(32) Strobl, G. *The Physics of Polymers*; Springer: Berlin, 2007.
(33) Magonov, S. N.; Cleveland, J.; Elings, V.; Denley, D.; Whangbo, M. H. *Surf. Sci.* **1997**, *389*, 201.
(34) Knoll, A.; Magerle, R.; Krausch, G. *Macromolecules* **2001**, *34*, 4159.
(35) Magonov, S. N.; Elings, V.; Whangbo, M. H. *Surf. Sci.* **1997**, *375*, L385.
(36) García, R.; Tamayo, J.; Paulo, A. S. *Surf. Interface Anal.* **1999**, *27*, 312.

MA8024464